

2D time-domain acoustic-elastic coupled modeling: a cell-based finite-difference method

Ho-Yong Lee *BK21, Division of Energy System Engineering, Seoul National University, Seoul 151-744, Republic of Korea*
Seung-Chul Lim *Department of Earth Science Education, Seoul National University, Seoul 151-748, Republic of Korea*
Dong-Joo Min* *Department of Energy Systems Engineering, Seoul National University, Seoul 151-744, Republic of Korea*
Byung-Doo Kwon *Department of Earth Science Education, Seoul National University, Seoul 151-748, Republic of Korea*
Minkyu Park *Korea Polar Research Institute (KOPRI), Songdo Techno Park, 7-50, Songdo-dong, Yeonsu-gu, Incheon 406-840, Republic of Korea*

ABSTRACT: To describe wave propagation in a fluid-solid environment which is usually encountered during marine seismic exploration, we design a time-domain acoustic-elastic coupled modeling algorithm based on the cell-based finite-difference method. The cell-based method has proven to delineate stress-free conditions correctly at the free surface with just changes in the material properties, which indicates that it can also properly deal with subsurface interface boundaries. In the acoustic-elastic coupled modeling, we first compose finite differences individually for the acoustic and elastic media; we then combine the differences using fluid-solid interface boundary conditions. Numerical experiments show that the cell-based coupled modeling algorithm gives solutions compatible with analytic solutions and that it properly describes S- and converted waves as well as P-waves. Applying the cell-based coupled modeling algorithm to a slope model, we confirm that our coupled modeling algorithm describes irregular interfaces properly, although it employs a staircase approximation of them.

Key words: acoustic-elastic coupled modeling, fluid-solid interface, cell-based, finite-difference method, time domain

1. INTRODUCTION

Fluid-solid environments are encountered in marine seismic exploration. While waves propagating in seawater are described by the acoustic wave equation, waves penetrating into the sea bottom are governed by the elastic wave equations. In conventional marine seismic exploration, pressure differences are measured by streamers, and the data are interpreted on the basis of acoustic wave propagation. The acoustic wave equation, however, is only valid for dealing with P-wave propagation, not for other S-waves and converted waves. Recently, the Ocean Bottom Cable (OBC) was developed, allowing for the acquisition of full-wave (multi-component) data in marine seismic exploration. This improved technology requires a correct description of elastic wave propagation below the sea bottom.

Acoustic wave equation can be derived from elastic wave

equations by defining the shear modulus as zero, which means that wave propagation in both acoustic and elastic media can be expressed solely with elastic wave equations. Accordingly, the staggered-grid finite-difference method (e.g., Virieux, 1986; Levander, 1988) for elastic wave equations has been used to describe wave propagation in fluid-solid coupled media. Discretization methods that only use displacements (called ‘purely displacement-based methods’ in this paper) cannot properly delineate fluid-solid coupled media in the same way as the staggered-grid method because they generate ringing noises around the source placed in the acoustic media (Choi et al., 2008). As a result, we individually apply acoustic and elastic wave equations to fluid and solid media and then combine the two regions using interface boundary conditions. There have been several studies on acoustic-elastic coupled media. Komatitsch et al. (2000) used the spectral-element method to simulate wave propagation in coupled media, and Zienkiewicz et al. (2005) depicted a finite-element coupled modeling algorithm. Choi et al. (2008) developed a frequency-domain waveform inversion algorithm for coupled media based on the finite-element method suggested by Zienkiewicz et al. (2005). Zhang (2004) pointed out that although both spectral-element and finite-element methods are flexible enough to describe irregular topographies, the finite-element method requires a great amount of computational effort, and the spectral-element method requires additional nodes to correctly describe the fluid-solid interface topography. Zhang (2004) proposed a coupled modeling algorithm using the grid method, which has about the same computer memory requirements as the second-order staggered-grid method, and it is flexible enough to describe irregular interfaces.

Considering that waveform inversion and reverse-time migration are the main applications of modeling algorithms, it is necessary to develop an efficient modeling algorithm that reduces computing time and computer core memory for acoustic-elastic coupled media. Although several methods

*Corresponding author: spoppy@snu.ac.kr

have been developed, the purely displacement-based finite-difference scheme still has its advantages, such as easy execution and less computational effort requirements than other methods of the same order (Min et al., 2004).

One of the main problems with conventional displacement-based finite-difference methods for elastic wave modeling is that they cannot properly describe stress-free conditions at the free surface, even when the additional free-surface boundary conditions are applied. To overcome this limitation, Min et al. (2004) developed the 2D cell-based finite-difference method for elastic media by defining material properties within cells rather than at nodal points. Min and Kim (2006) applied the cell-based method to 3D time-domain elastic wave modeling. In doing so, they were able to properly describe the free-surface boundary and satisfy the reciprocity theorem. By introducing the cell-based method and the appropriate interface boundary conditions in coupled media, we can develop an effective modeling algorithm for coupled media.

Seismic wave modeling has been carried out in time and frequency domains. The advantages of time-domain modeling algorithms are that they are easy to carry out, and the computer memory requirements are not as great as frequency-domain modeling algorithms. One well-known weakness of time-domain modeling algorithms is that the same procedures need to be repeated whenever the source position changes, even for the same model (Jo et al., 1996; Min et al., 2000, 2003). This weakness, which can lead to increasing computation times for models with multiple sources, can be overcome by parallel computing. On the other hand, frequency-domain modeling algorithms require a great amount of computer core memory because of the storage needed for the complex impedance matrix. Although frequency-domain modeling algorithms are more efficient than time-domain algorithms for models with multiple sources or with viscoelastic attenuation features (Min et al., 2000, 2003, 2004; Pratt, 1990), they may not be appropriate for large and complicated models, such as 3D models.

In this study, we present a time-domain acoustic-elastic coupled modeling algorithm on the basis of a purely displacement-based finite-difference method. Our acoustic-elastic coupled modeling algorithm is constructed by introducing the cell-based method proposed by Min et al. (2004) to discretize acoustic and elastic wave equations. We also incorporate boundary conditions suggested by Zhang (2004) into the modeling algorithm to correctly describe the interfaces between fluid and solid media. We verify our coupled modeling algorithm by comparing numerical solutions to analytic solutions for simple acoustic-elastic coupled media, as done by Komatitsch et al. (2000) and Choi et al. (2008). To validate the accuracy of our algorithm, we also compare numerical solutions generated by the cell-based coupled modeling algorithm to those of the conventional node-based coupled modeling algorithm. We apply our algorithm to a

horizontal three-layer and a slope model to examine whether the coupled algorithm correctly describes converted waves as well as reflections.

2. WAVE EQUATIONS FOR ACOUSTIC-ELASTIC COUPLED MEDIA

In acoustic-elastic coupled media, a fluid layer is overlaid on solid layers. Waves propagating through the fluid layer can be described with the acoustic wave equation as

$$\frac{1}{k} \frac{\partial^2 P}{\partial t^2} = \frac{\partial}{\partial x} \left(\frac{1}{\rho_f} \frac{\partial P}{\partial x} \right) + \frac{\partial}{\partial z} \left(\frac{1}{\rho_f} \frac{\partial P}{\partial z} \right) \quad (1)$$

where P is the pressure, ρ_f is the density of the fluid layer, and k indicates incompressibility. When acoustic waves meet the fluid-solid interfaces, they are converted into elastic waves. In this case, P- and S-waves and their converted waves are generated. Under the fluid-solid interfaces, waves are delineated by the elastic wave equations, expressed as

$$\rho \frac{\partial^2 u}{\partial t^2} = \frac{\partial \sigma_{xx}}{\partial x} + \frac{\partial \sigma_{xz}}{\partial z} \quad (2)$$

$$\rho \frac{\partial^2 w}{\partial t^2} = \frac{\partial \sigma_{zz}}{\partial z} + \frac{\partial \sigma_{xz}}{\partial x} \quad (3)$$

$$\sigma_{xx} = (\lambda + 2\mu) \frac{\partial u}{\partial x} + \lambda \frac{\partial w}{\partial z} \quad (4)$$

$$\sigma_{zz} = (\lambda + 2\mu) \frac{\partial w}{\partial z} + \lambda \frac{\partial u}{\partial x} \quad (5)$$

$$\sigma_{xz} = \sigma_{zx} = \mu \left(\frac{\partial u}{\partial z} + \frac{\partial w}{\partial x} \right) \quad (6)$$

where u and w are the horizontal and vertical displacements, λ and μ are the Lamé constants, and σ is the stress.

In order to combine the two governing equations at the interfaces, we need boundary conditions so that the normal traction and the normal components of particle velocity are continuous across the interfaces. At the interfaces, we can express the relationship between pressure and stresses (Zhang 2004) as

$$-Pl = \sigma_{xx}l + \sigma_{xz}m \quad (7)$$

$$-Pm = \sigma_{zz}m + \sigma_{xz}l \quad (8)$$

where l and m are the direction cosines of the normal vector to the fluid-solid interfaces. Combining Equations (7) and (8) yields

$$-P(l^2 + m^2) = l^2 \sigma_{xx} + 2lm \sigma_{xz} + m^2 \sigma_{zz}. \quad (9)$$

The continuity of the normal components of particle velocity

across the interfaces gives

$$-\frac{1}{\rho} \left(\frac{\partial P}{\partial x} l + \frac{\partial P}{\partial z} m \right) = \frac{\partial^2 u}{\partial t^2} l + \frac{\partial^2 w}{\partial t^2} m. \quad (10)$$

From Equations (9) and (10), we note that when acoustic waves meet the fluid-solid interfaces, horizontal and vertical displacements in the elastic medium are generated by the changes of pressure in the acoustic medium. On the other hand, when the elastic waves bump the fluid-solid interfaces, normal and shear stresses (or horizontal and vertical displacements) in the elastic medium are converted into pressure in the acoustic medium.

When the interface boundary is horizontal, stresses σ_{xx} and σ_{xz} ($=\sigma_{zx}$) disappear, which simplifies the interface boundary conditions as follows

$$-P = \sigma_{zz} = (\lambda + 2\mu) \frac{\partial w}{\partial z} + \lambda \frac{\partial u}{\partial x} \quad (11)$$

$$\rho_f \frac{\partial^2 w}{\partial t^2} = -\frac{\partial P}{\partial z}. \quad (12)$$

For the vertical interface boundary, stresses σ_{zz} and σ_{xz} ($=\sigma_{zx}$) disappear, which yields

$$-P = \sigma_{xx} = (\lambda + 2\mu) \frac{\partial u}{\partial x} + \lambda \frac{\partial w}{\partial z} \quad (13)$$

$$\rho_f \frac{\partial^2 u}{\partial t^2} = \frac{\partial P}{\partial x}. \quad (14)$$

For horizontal or vertical interfaces, either vertical or horizontal displacements are generated from pressure differences, and those differences are generated by σ_{zz} or σ_{xx} . Using these relationships, we can combine the pressure in acoustic media and the displacements in elastic media.

3. FINITE DIFFERENCES FOR COUPLED WAVE EQUATIONS

We composed finite differences for the acoustic and elastic wave equations and the interface boundary conditions using the cell-based finite-difference method suggested by Min et al. (2004). In the conventional node-based finite-difference method, both displacements and material properties are assigned to nodal points, whereas in the cell-based method, material properties are defined within cells (e.g., Fig. 1). Min et al. (2004) demonstrated that the cell-based method properly addresses the stress-free boundary condition at the free surface with just the changes of material properties in elastic media. This means that we can correctly delineate elastic wave propagation with a purely displacement-based finite-difference method when we use the cell-based method. It leads us to apply the cell-based, rather than node-based, finite-difference method to the acoustic-

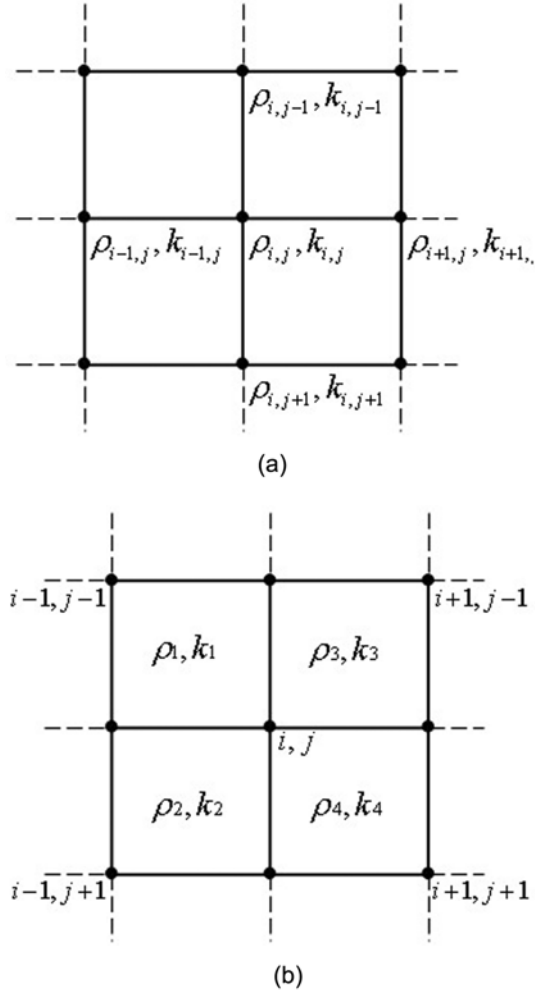


Fig. 1. (a) The conventional node-based and (b) cell-based grid sets used to obtain the finite difference solution at the (i, j) th nodal point.

elastic coupled modeling.

In the cell-based grid set (e.g., Fig. 1b), the acoustic wave equation is approximated by

$$\frac{1}{k} \frac{\partial^2 P}{\partial t^2} \approx \frac{1}{4} \left(\frac{1}{k_1} + \frac{1}{k_2} + \frac{1}{k_3} + \frac{1}{k_4} \right) \frac{P_{i,j}^{n+1} - 2P_{i,j}^n + P_{i,j}^{n-1}}{(\Delta t)^2} \quad (15)$$

$$\frac{\partial}{\partial x} \left(\frac{1}{\rho} \frac{\partial P}{\partial x} \right) \approx \frac{1}{(\Delta x)^2}$$

$$\left[\frac{1}{2} \left(\frac{1}{\rho_3} + \frac{1}{\rho_4} \right) (P_{i+1,j}^n - P_{i,j}^n) - \frac{1}{2} \left(\frac{1}{\rho_1} + \frac{1}{\rho_2} \right) (P_{i,j}^n - P_{i-1,j}^n) \right] \quad (16)$$

$$\frac{\partial}{\partial z} \left(\frac{1}{\rho_f} \frac{\partial P}{\partial z} \right) \approx \frac{1}{(\Delta z)^2}$$

$$\left[\frac{1}{2} \left(\frac{1}{\rho_2} + \frac{1}{\rho_4} \right) (P_{i,j+1}^n - P_{i,j}^n) - \frac{1}{2} \left(\frac{1}{\rho_1} + \frac{1}{\rho_3} \right) (P_{i,j}^n - P_{i,j-1}^n) \right] \quad (17)$$

where k represents the incompressibility and $k_1, k_2, k_3,$ and

k_4 indicate the incompressibility for the adjacent cells surrounding the (i, j) th nodal point. Because the incompressibility is not assigned to the (i, j) th point in the cell-based grid set (Fig. 1b), we use the averages of compressibility values of the four adjacent cells to describe the compressibility $(1/k)$ at the (i, j) th nodal point as shown in Equation (15).

Finite differences for the elastic wave equations are expressed by

$$\rho \frac{\partial^2 u}{\partial t^2} \approx \frac{1}{4}(\rho_1 + \rho_2 + \rho_3 + \rho_4) \frac{u_{i,j}^{n+1} - 2u_{i,j}^n + u_{i,j}^{n-1}}{(\Delta t)^2} \quad (18)$$

$$\frac{\partial}{\partial x} \left(a \frac{\partial u}{\partial x} \right) \approx \frac{1}{(\Delta x)^2}$$

$$\left[\frac{1}{2}(a_3 + a_4)(u_{i+1,j}^n - u_{i,j}^n) - \frac{1}{2}(a_1 + a_2)(u_{i,j}^n - u_{i-1,j}^n) \right] \quad (19)$$

$$\frac{\partial}{\partial z} \left(a \frac{\partial u}{\partial z} \right) \approx \frac{1}{(\Delta z)^2}$$

$$\left[\frac{1}{2}(a_2 + a_4)(u_{i,j+1}^n - u_{i,j}^n) - \frac{1}{2}(a_1 + a_3)(u_{i,j}^n - u_{i,j-1}^n) \right] \quad (20)$$

$$\frac{\partial}{\partial x} \left(a \frac{\partial u}{\partial z} \right) \approx \frac{1}{4\Delta x \Delta z}$$

$$\left[\begin{array}{l} a_1 u_{i-1,j-1}^n + (a_1 - a_3) u_{i,j-1}^n - a_3 u_{i+1,j-1}^n \\ + (a_2 - a_1) u_{i-1,j}^n + (a_3 - a_1 + a_2 - a_4) u_{i,j}^n + (a_3 - a_4) u_{i+1,j}^n \\ - a_2 u_{i-1,j+1}^n + (a_4 - a_2) u_{i,j+1}^n + a_4 u_{i+1,j+1}^n \end{array} \right] \quad (21)$$

$$\frac{\partial}{\partial z} \left(a \frac{\partial u}{\partial x} \right) \approx \frac{1}{4\Delta x \Delta z}$$

$$\left[\begin{array}{l} a_1 u_{i-1,j-1}^n + (a_3 - a_1) u_{i,j-1}^n - a_3 u_{i+1,j-1}^n \\ + (a_1 - a_2) u_{i-1,j}^n + (a_3 - a_1 + a_2 - a_4) u_{i,j}^n + (a_4 - a_3) u_{i+1,j}^n \\ - a_2 u_{i-1,j+1}^n + (a_2 - a_4) u_{i,j+1}^n + a_4 u_{i+1,j+1}^n \end{array} \right] \quad (22)$$

where a indicates elastic constants. For the water surface boundary, the Dirichlet boundary condition should be applied (Officer, 1958). The finite differences for the fluid-solid interface boundary conditions are written from Equations (9) and (10) as

$$-P_{i,j}(l^2 + m^2) = l^2 \sigma_{xx,ij} + 2lm \sigma_{xz,ij} + m^2 \sigma_{zz,ij} \quad (23)$$

with

$$\sigma_{xx,ij} = (\lambda + 2\mu) \frac{u_{i+1,j}^n - u_{i,j}^n}{\Delta x} + \lambda \frac{u_{i,j+1}^n - w_{i,j}^n}{\Delta z} \quad (24)$$

$$\sigma_{zz,ij} = (\lambda + 2\mu) \frac{w_{i,j+1}^n - w_{i,j}^n}{\Delta z} + \lambda \frac{u_{i,j+1}^n - u_{i,j}^n}{\Delta x} \quad (25)$$

$$\sigma_{xz,ij} = \sigma_{zx,ij} = \mu \left(\frac{u_{i,j+1}^n - u_{i,j}^n}{\Delta z} + \frac{w_{i+1,j}^n - w_{i,j}^n}{\Delta x} \right) \quad (26)$$

and

$$\begin{aligned} & -\frac{1}{\rho_f} \left(\frac{P_{i+1,j}^n - P_{i,j}^n}{\Delta x} l + \frac{P_{i,j+1}^n - P_{i,j}^n}{\Delta x} m \right) \\ & = l \frac{u_{i,j+1}^{n+1} - 2u_{i,j}^n + u_{i,j}^{n-1}}{(\Delta t)^2} + m \frac{u_{i,j}^{n+1} - 2w_{i,j}^n + w_{i,j}^{n-1}}{(\Delta t)^2} \end{aligned} \quad (27)$$

where material properties should be discretized in the same manner as for the main body. We do not specify the discretization for material properties because they are dependent on the shape of interfaces.

In order to suppress the unwanted edge reflections, we applied the absorbing boundary conditions suggested by Reynolds (1978) and Higdon (1991) to acoustic and elastic media, respectively.

4. NUMERICAL EXAMPLES

We verified our acoustic-elastic coupled modeling algorithm by first comparing numerical solutions obtained by our cell-based coupled modeling algorithm to analytic solutions. The analytic solution is described in Ewing et al. (1957). We assumed a simple fluid-solid model as shown in Figure 2. In the model, a fluid layer overlies a homogeneous solid layer, and a source is excited at a depth of 20 m under the fluid surface. For the source wavelet, we applied the first derivative of a Gaussian function, which had a maximum frequency of 20 Hz. Since we used the second-order finite-difference schemes, we required more than 21.6 grid points per wavelength for acoustic wave equations and more than 33.3 grid points per shear wavelength for elastic wave equations; this was necessary to bound errors within 1% in reference to group velocity (Marfurt, 1984; Min et al., 2000). In such case, we needed to use a grid interval smaller than 2.5 m to obtain reliable solutions. This was computed by $\lambda_{\min} = v_{\min} / f_{\max}$ and $\lambda_{\min} = G\Delta$ (λ : wavelength, v : velocity, f : frequency, Δ : grid interval, and G is the number of grid points per minimum wavelength). The time interval was determined to be 0.001 s by considering the stability conditions. Figure 3 shows the analytic and numerical solutions obtained by our cell-based coupled modeling algorithm at receiver 1 (placed in a fluid region in Fig. 2). For comparison, we also display numerical solutions generated by conventional node-based coupled modeling techniques. Since the finite-difference operators of the node-based method for the acoustic and elastic wave equations are well known, we do not describe them in this paper. Finite-difference operators for the interface boundary conditions are similar to those of the cell-based method, except for the discretization of material properties. In Figure 3, we can see that the numerical solutions computed by our cell-based coupled modeling algorithm

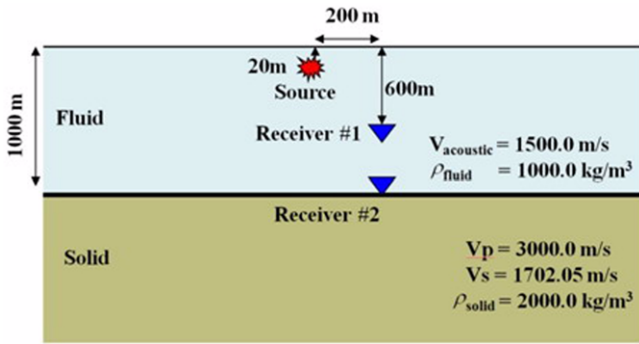


Fig. 2. The geometry of the simple fluid-solid coupled model.

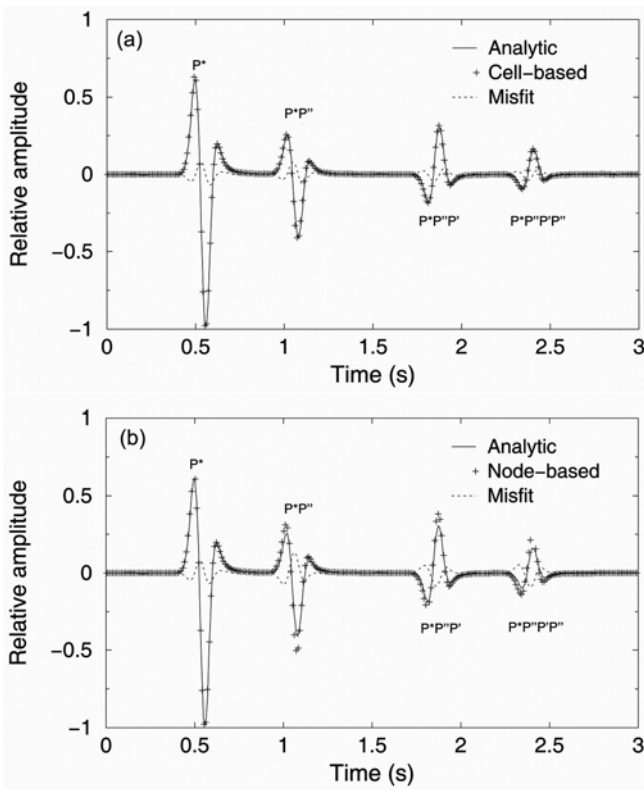


Fig. 3. Comparison of analytic and numerical solutions obtained by (a) the cell-based and (b) the node-based finite-difference methods at receiver 1 of Figure 2: P*, P', and P'' represent the direct waves, the waves reflected at the water surface, and the waves reflected at the interfaces, respectively.

are in good agreement with the analytic solutions, while those by the node-based coupled modeling show larger amplitudes than the analytic solutions. In Figure 4, we display numerical solutions recorded at the interface by the cell-based and node-based coupled modeling algorithms. Pressures obtained by the node-based method are larger than those of the cell-based method, while vertical displacements show the reverse. Consequently, such deviations may result in incorrect solutions, as shown in Figure 3. From these results, we note that the cell-based coupled modeling algorithm can

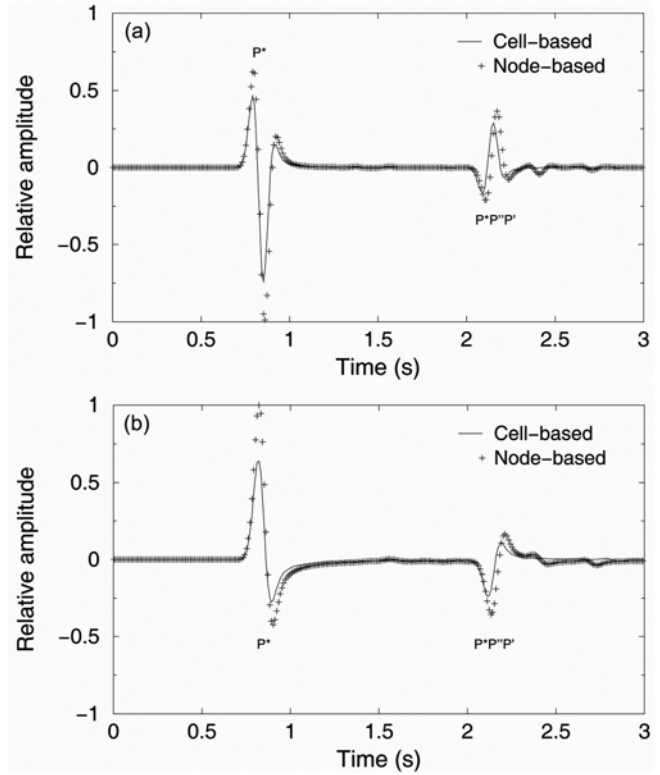


Fig. 4. Comparison of numerical solutions for pressure (a) and vertical displacements (b) obtained by the cell-based (solid line) and node-based (plus symbols) finite-difference methods at receiver 2 of Figure 2: P*, P', and P'' represent the direct waves, the waves reflected at the water surface, and the waves reflected at the interfaces, respectively.

provide more reliable solutions for fluid-solid coupled media than the node-based coupled modeling algorithm. In order to show how waves generated by pressure differences propagate through the solid layer, we display pressures and vertical displacements together on the same snapshot (Fig. 5). However, the amplitude of pressure is much larger than that of displacement, which makes the displacements invisible in the snapshot. To make a better display, we scaled displacements by a constant only to balance them with pressure.

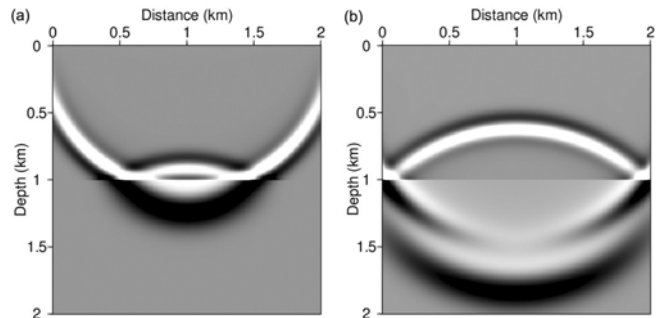


Fig. 5. Snapshots of pressures (above the interface boundary) and vertical displacements (under the interface boundary) at (a) 0.425 s and (b) 0.525 s.

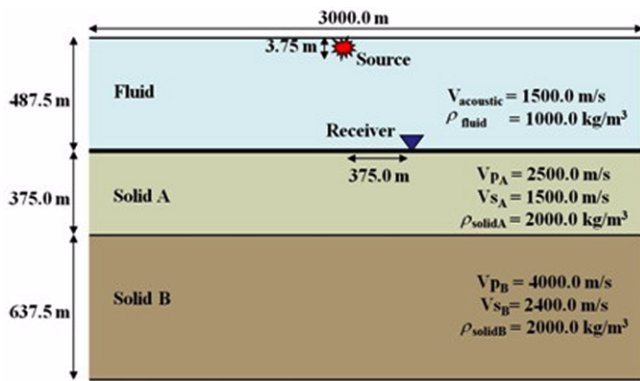


Fig. 6. The geometry of the three-layered model.

We proceeded to examine whether the acoustic-elastic coupled modeling algorithm depicts S- and converted waves. We applied the acoustic-elastic coupled modeling algorithm to the horizontal three-layer model (Fig. 6). The source, which had a maximum frequency of 40 Hz, was exploded at a depth of 3.75 m under the fluid surface. Considering numerical dispersion conditions, we required a grid interval smaller than 1.125 m. Because we worked with a Linux system installed on a 2.4 GHz Pentium 4 with 1 Gb of RAM, we suffered from computer memory limitations. This led us to use a grid interval of 3.75 m and 801×401 grid points to simulate the model. The time interval was

0.0005 s. We placed 801 receivers at the fluid-solid interface. In Figure 7, we show seismograms generated by the pure-acoustic and acoustic-elastic coupled modeling algorithms at the receivers. From Figure 7, we find that the acoustic wave-modeling algorithm did not generate any converted waves, while the acoustic-elastic coupled modeling algorithm successfully generated P-S and S-P converted waves. In Figure 8, we compare traces of the pressure seismograms recorded at the receiver shown in Figure 6. In this

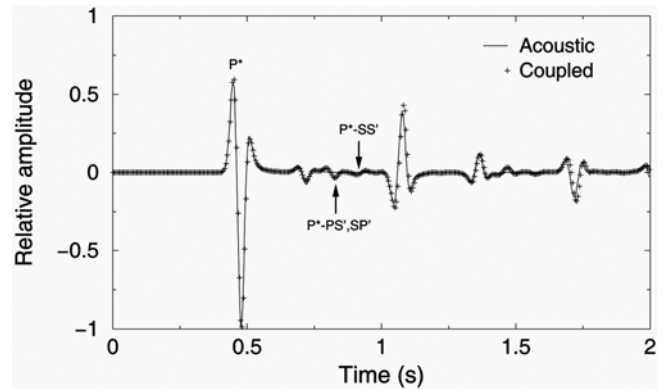


Fig. 8. Comparison of numerical solutions obtained by the cell-based coupled modeling (plus symbols) and pure-acoustic wave modeling (solid line) algorithms at the receiver of Figure 6: The superscripts * and ' denote the direct wave and the reflected wave, respectively. The dash (-) indicates the interface.

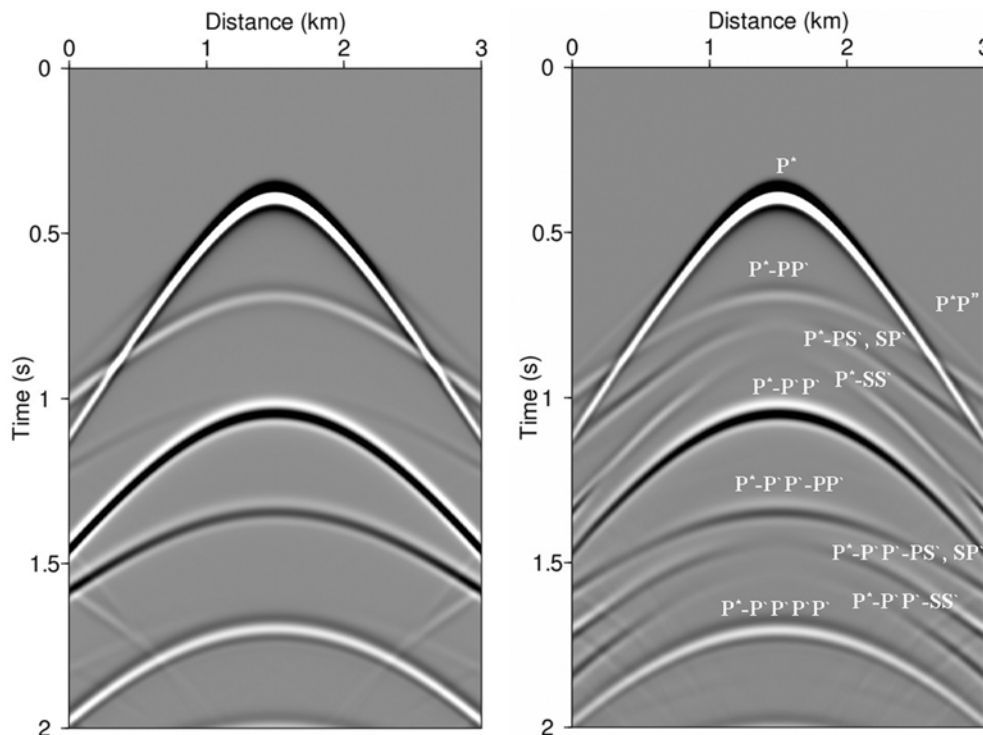


Fig. 7. Seismograms for pressures computed by (a) the pure-acoustic and (b) the acoustic-elastic coupled modeling algorithm at 801 receivers located along the fluid-solid interface in Figure 6: The superscripts *, ', and " denote the direct wave, the reflected wave, and the refracted wave, respectively. The dash (-) indicates the interface.

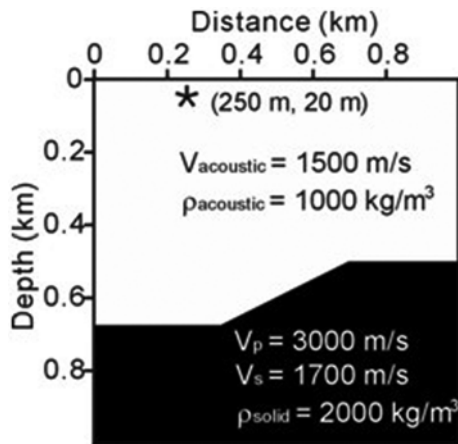


Fig. 9. The geometry of the slope model.

figure, we can also observe several converted waves.

Next we investigated the feasibility of our algorithm on irregular interfaces. We used a slope model, as shown in Figure 9. We employed a staircase approximation for the slope interface. In this case, we obtained nearly correct solutions as long as the staircases did not cause any artificial effects (i.e., as long as the grid size was small enough). The dimensions of the slope model were $1,000 \text{ m} \times 1,000 \text{ m}$. For the source, we applied the first derivative of the Gaussian function with a maximum frequency of 80 Hz at a depth of 20 m. We employed a grid interval of 2.5 m and a time interval of 0.0005 s. Figure 10 shows snapshots for pressure and displacements. We made normalization between the displacements and pressure by multiplying a certain value. Figure 11 shows seismograms for the pressure recorded at a depth of 200 m. From Figures 10 and 11, it is evident that our coupled modeling algorithm can properly describe irregular topography.

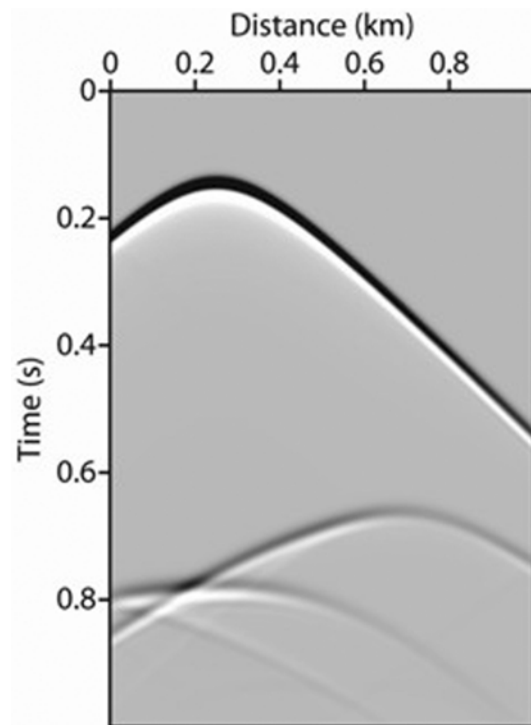


Fig. 11. Seismogram of pressure recorded at a depth of 200 m from the surface.

5. CONCLUSIONS

We developed a time-domain acoustic-elastic coupled modeling algorithm based on the cell-based finite-difference method. The cell-based method has proven to yield correct solutions for elastic media, even though it only employs displacements. In the acoustic-elastic modeling algorithm, we first composed finite differences individually for the acoustic and elastic media. We then combined the finite differences using the interface boundary conditions.

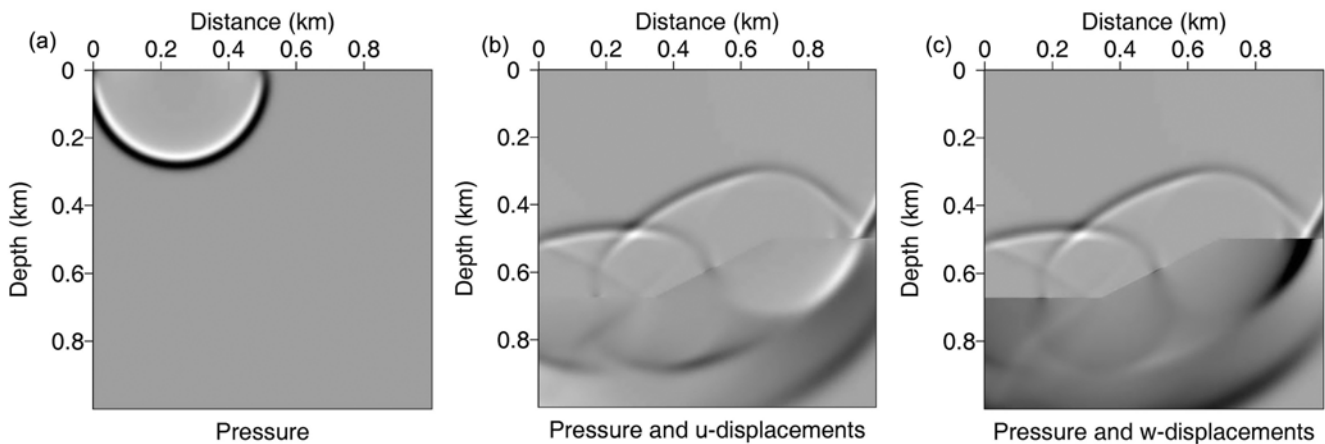


Fig. 10. Snapshots of pressure (above the interface) and displacements (below the interface) at (a) 0.2 s, and (b and c) 0.6 s: (a) pure pressure, (b) pressure and horizontal displacements, and (c) pressure and vertical displacements.

Comparing the analytic and numerical solutions, we found that the cell-based coupled modeling algorithm yielded more accurate solutions than the conventional node-based coupled modeling algorithm. We also confirmed that the acoustic-elastic coupled modeling properly described S- and converted waves, as well as P-waves. After applying the cell-based coupled modeling algorithm to a slope model, we noted that the modeling algorithm can also appropriately simulate irregular topography. Considering the well-known advantages of pure displacement-based finite-difference modeling techniques that are simple to carry out and require less computer memory, our algorithm can be practical for seismic waveform inversion.

ACKNOWLEDGMENTS: This work was financially supported by Brain Korea 21 project of Ministry of Education, Science and Technology, KOPRI grant PP09020 and PM09030, and Research Settlement Fund for the new faculty of Seoul National University.

REFERENCES

- Choi, Y., Min, D.-J., and Shin, C., 2008, Two-dimensional waveform inversion of multi-component data in acoustic-elastic coupled media. *Geophysical prospecting*, 56, 863–881.
- Ewing W.M., Jardetzky W.S., and Press F., 1957, *Elastic waves in layered media*. McGraw-Hill, New York, 175 p.
- Higdon, R.L., 1991, Absorbing boundary conditions for elastic waves. *Geophysics*, 56, 231–241.
- Jo, C.-H., Shin, C., and Suh, J.H., 1996, An optimal 9-point, finite-difference, frequency-space, 2-D scalar wave extrapolator. *Geophysics*, 61, 529–537.
- Komatitsch, D., Barnes, C., and Tromp, J., 2000, Wave propagation near a fluid-solid interface: A spectral-element approach. *Geophysics*, 65, 623–631.
- Levander, A.R., 1988, Fourth-order finite-difference P-SV seismograms. *Geophysics*, 53, 1425–1436.
- Marfurt, K.J., 1984, Accuracy of finite-difference and finite-element modeling of the scalar and elastic wave equations. *Geophysics*, 49, 533–549.
- Min, D.-J., Shin, C., Kwon, B.-D., and Chung, S., 2000, Improved frequency-domain elastic wave modeling using weighted-averaging difference operators. *Geophysics*, 65, 884–895.
- Min, D.-J., Shin, C., Pratt, R.G., and Yoo, H.S., 2003, Weighted-averaging finite-element method for 2D elastic wave equations in the frequency domain. *Bulletin of the Seismological Society of America*, 93, 904–921.
- Min, D.-J. and Kim, H.-S., 2006, Feasibility of the surface-wave method for the assessment of physical properties of a dam using numerical analysis. *Journal of Applied Geophysics*, 59, 236–243.
- Min, D.-J., Shin, C., and Yoo, H.S., 2004, Free-Surface Boundary Condition in Finite-Difference Elastic Wave Modeling. *Bulletin of the Seismological Society of America*, 94, 237–250.
- Officer, C.B., 1958, *Introduction to the theory of sound transmission: With application to the ocean*. McGraw-Hill, New York, p. 110-115.
- Pratt, R.G., 1990, Frequency-domain elastic wave modeling by finite differences: A tool for crosshole seismic imaging. *Geophysics*, 55, 626–632.
- Reynolds, A.C., 1978, Boundary conditions for the numerical solution of wave propagation problems. *Geophysics*, 43, 1099–1110.
- Virieux, J., 1986, P-SV wave propagation in heterogeneous media: Velocity-stress finite-difference method. *Geophysics*, 51, 889–899.
- Zhang, J., 2004, Wave propagation across fluid-solid interfaces: a grid method approach. *Geophysical Journal International*, 159, 240–252.
- Zienkiewicz O.C., Taylor R.L., and Zhu, J.Z., 2005, *The finite element method: Its basis & fundamentals*. Elsevier, Oxford, p. 634–637.

Manuscript received April 15, 2009

Manuscript accepted October 20, 2009